

J. W. Fowler<sup>1</sup>, W. B. Doriese<sup>1</sup>, G. Hilton<sup>1</sup>,  
K. Irwin<sup>1</sup>, D. Schmidt<sup>1</sup>, G. Stiehl<sup>1</sup>, D. Swetz<sup>1</sup>,  
J. N. Ullom<sup>1</sup>, and L. Vale<sup>1</sup>

# Optimization and analysis of code-division multiplexed TES microcalorimeters

22.07.2011

**Keywords** SQUID multiplexers, transition edge sensors

**Abstract** We are developing code-division multiplexing (CDM) systems for TES arrays with the goal of reaching multiplexing factors in the hundreds. We report on x-ray measurements made with a four-channel prototype CDM system that employs a flux-summing architecture, emphasizing data-analysis issues. We describe an empirical method to determine the demodulation matrix that minimizes cross-talk. This CDM system achieves energy resolutions of between 2.3 eV and 3.0 eV FWHM at 5.9 keV.

PACS numbers: 85.25.Dq, 85.25.Oj

## 1 Introduction

Transition-edge sensors<sup>1</sup> (TESs) are used in many different applications to sense photons over an enormous energy range. They are the leading detector technology in millimeter-wave and submillimeter astronomy, where focal planes of thousands of sensors have been fielded<sup>2,3</sup> and show great promise for astronomical x-ray spectroscopy. In the laboratory, TES devices have achieved the best energy resolution of any non-dispersive device for single photons in the gamma and x-ray bands—better than one part in one thousand.

One critical technology for building arrays of thousands of detectors has been cryogenic signal multiplexing, which reduces the number of electrical connections between stages at different temperatures by allowing multiple detectors to share

---

1:Quantum Sensors Project, National Institute of Standards and Technology, 325 Broadway MS 817.03, Boulder, CO 80305, USA  
Tel: +1 303-497-3990  
E-mail: joe.fowler@nist.gov  
*Official contribution of the National Institute of Standards and Technology; not subject to copyright in the United States.*

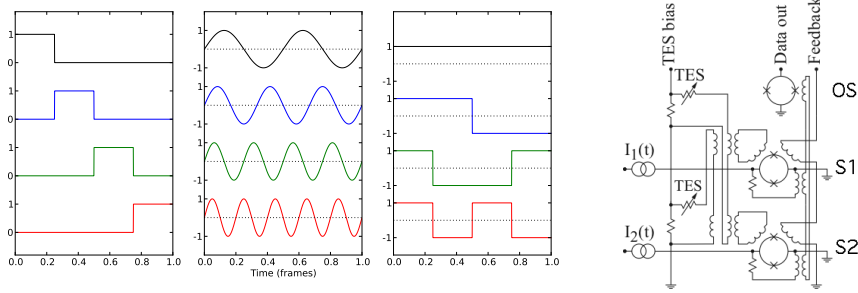


**Fig. 1** (Color online) *Left*: Three sets of orthogonal basis functions for multiplexing four pixels: time-division (boxcars), frequency-division (sinusoids), and code-division (Walsh codes). In each multiplexing scheme, the four detector outputs are multiplied by one of the four given modulation functions. *Right*: A two-channel code-division multiplexer that uses flux summation. Labels “OS”, “S1”, and “S2” refer to the output SQUID and SQUID switches 1 and 2. The magnetic flux in SQUID switch 1 is proportional to the sum of the two TES currents, while the flux in switch 2 is proportional to their difference (indicated by the oppositely-oriented inductors). When current is applied at either  $I_1(t)$  or  $I_2(t)$ , the output SQUID couples to either the sum or the difference of TES currents. We report on this CDM design, generalized to four TES detectors and an equal number of SQUID switches.

wiring. As future projects grow to larger device counts and employ faster detectors, they will require new multiplexing techniques to minimize both readout noise and instrument complexity.

Two multiplexing schemes currently used with TES arrays are time-division multiplexing (TDM)<sup>4</sup> and frequency-division multiplexing (FDM).<sup>5</sup> In this work, we present the first x-ray measurements with TES microcalorimeters read out with code-division multiplexing (CDM). This multiplexing approach combines many advantages of the other two, as argued in earlier works.<sup>6,7</sup> Figure 1 (left panel) compares the modulation functions used in TDM, FDM, and CDM for a four-channel system. In TDM, one detector is coupled to the output at a time. In CDM, all detectors are coupled at all times—with time-varying signs—removing the “multiplex disadvantage” of TDM, in which the aliased SQUID noise increases as the square root of  $N$ , the number of multiplexed detectors. CDM therefore has the potential to permit higher device speed, or to increase the number of devices multiplexed on one line, or both. We describe the design and characterization of a four-channel prototype and demonstrate that the energy resolution achieved while measuring 5.9 keV x-rays matches the resolution achieved through TDM readout.

## 2 A 4-channel CDM demonstration system

We have measured x-rays with microcalorimeters optimized for the 1 to 10 keV energy range, read out through a demonstration chip fabricated at NIST containing a four-channel CDM circuit. The code-division multiplexer operates by the principle of flux summation.<sup>8</sup> The right panel of Figure 1 shows a simplified two-channel model of the multiplexer. As in a TDM system,  $N$  detectors couple their current into  $N$  switching SQUIDs, whose outputs are summed by a single output SQUID. In a TDM system, the detectors and switching SQUIDs are paired so that

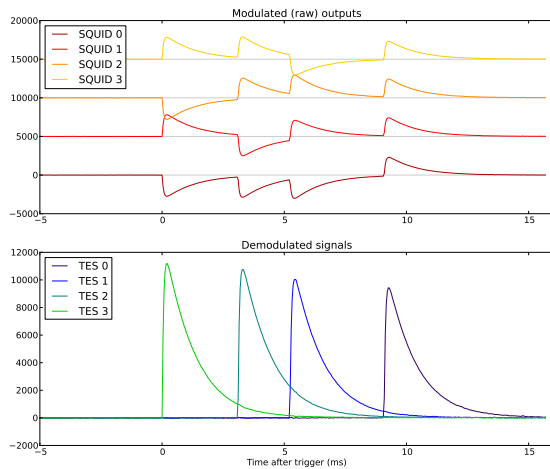


**Fig. 2** (Color online) Sample data from observing manganese fluorescence light for 21 ms. The raw data from the four SQUID switches (*top*) and the same data demodulated to recover the current from each of the four TES detectors (*bottom*) are shown. The vertical scale is arbitrary; the upper panel offsets each curve for clarity. This unusual time interval was selected to demonstrate all four modulations in one figure; only a small fraction of pulse records contain even two photons coinciding in such a short window.

each detector couples into only one switching SQUID; in the CDM system, all  $N$  detectors couple into all  $N$  SQUIDs, each detector having a different pattern of positive and negative couplings. For an appropriate set of  $N^2$  coupling polarities, the detectors' patterns are mutually orthogonal over the period required to read all  $N$  switching SQUIDs. The Walsh functions<sup>9</sup> provide one such basis.

The TDM and flux-summed CDM systems are used identically; in both, the  $N$  SQUID switches are activated singly in rapid succession. We can therefore use CDM chips as drop-in replacements for the TDM, with identical warm electronics to multiplex the signals. This interchangeability has enabled both rapid testing of the CDM prototype and direct comparisons of CDM with TDM results.

### 3 Characterization of the CDM data

We used CDM to read out a TES array measuring x-rays emitted by a manganese target bombarded with wide-band brehmsstrahlung radiation. Manganese fluoresces with a pair of  $K\alpha$  lines<sup>10</sup> at 5.9 keV separated by 11.1 eV. We estimate the energy resolution of the calorimeters from the observed line shapes.

Figure 2 shows a brief excerpt of the data from the 4-channel CDM system. The top panel shows the raw data as recorded by the system, one record from each of the four switching SQUIDs. They have been modulated by the Walsh functions designed into the CDM chip. Inversion of the Walsh coding yields the separate TES currents—as shown in the bottom panel of Figure 2.

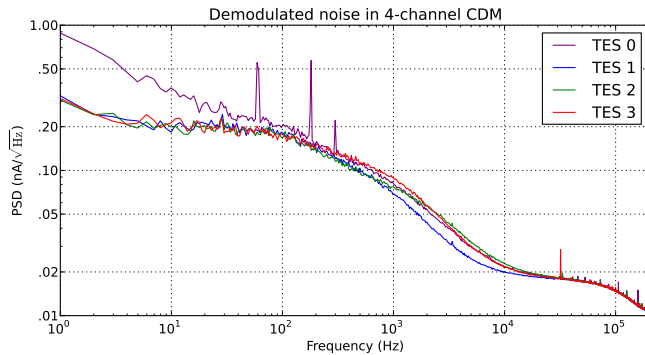


**Fig. 3** (Color online) The square root of the noise power spectral density in demodulated four-channel CDM data, averaged over 90 seconds with no x-ray sources. TES 0—the one unmodulated detector—has the highest noise level below 200 Hz, owing to gain drifts in second and third stage SQUIDs and pickup of the 60 Hz AC power line frequency (and at two odd harmonics). Modulation by Walsh functions removes most of this extra noise from the signal band in the other detector channels. The in-frame linear time correction described in Section 3.2 suppresses noise above 100 kHz in all channels.

One advantage of modulation by Walsh functions is that all but one detectors’ signals are differenced at multiples of the modulation frequency. Upon demodulation, low-frequency drifts and noise at the AC power line frequency and its overtones are moved out of the signal band, provided their source is upstream of the modulator (such as in the warm electronics). This effect can be seen in Figure 3, where only TES 0 (the unmodulated device) has excess noise below 100 Hz.

### 3.1 Solving for the demodulation matrix

One challenge in CDM is computation of the true demodulation matrix  $\mathbf{D}$  required to find the current through each of the  $N$  detectors given the  $N$  multiplexed outputs. We define  $D_{ij}$  as the contribution of the current from TES  $i$  to output channel  $j$ . By design, this matrix consists entirely of  $+1$  and  $-1$  elements:

$$\mathbf{D} = \begin{bmatrix} 1 & 1 & 1 & 1 \\ -1 & 1 & 1 & -1 \\ -1 & -1 & 1 & 1 \\ -1 & 1 & -1 & 1 \end{bmatrix} \quad (1)$$

In flux-summed CDM, the modulation coefficients are wired into the design by the lithographic traces in the multiplexer and cannot be adjusted after fabrication. Because the exact couplings depend on details of the SQUID switches and the geometry of the coils that convert current into magnetic flux,  $\mathbf{D}$  differs somewhat from its design value. We estimate the matrix empirically and have found that it is consistent over many weeks of operation. When needed, it can be computed from any sufficiently long calibration data set.

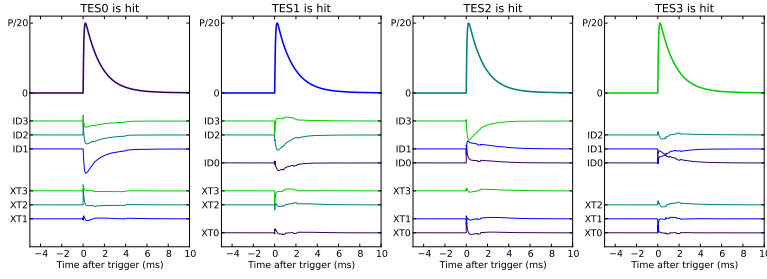


**Fig. 4** (Color online) Reduction in cross-talk through refining the demodulation matrix. Each panel shows the pulses caused by the TES cited at the top. The highest curve shows the pulse shape for the primary signal, scaled down by a factor of 20 for better comparison to cross-talk. Below this, three curves labeled “ID” show the unwanted cross-talk response in the *other* three channels, assuming an integer-only demodulation matrix. The lowest three curves show the cross-talk (“XT”) when the empirically derived demodulation is applied instead.

We refine our estimate of  $\mathbf{D}$ , starting from the integer-only matrix (Equation 1). The data required for the refinement are the mean current signals  $s_{ij}(t)$  from demodulated channel  $i$  when device  $j$  (and no other) is hit with a photon, plus the noise power spectrum  $n_j$  of each device. Figure 4 shows an example of all sixteen signals with the  $i = j$  cases plotted in the top of each panel and the twelve cross-talk ( $i \neq j$ ) cases below. The sampled functions of time are each converted to single values by the usual process of optimal filtering. A correction matrix  $\mathbf{C}$  is built from the filtered values:  $C_{ij}$  is the response in channel  $i$  to a photon hitting detector  $j$ . The correction  $\mathbf{C}$  will be close to the identity if  $\mathbf{D}$  was a good initial estimate. The revised demodulation matrix is then  $\mathbf{D}' = \mathbf{C}^{-1} \mathbf{D}$ . In practice, we find that elements of  $\mathbf{D}'$  are generally within 1% of  $\pm 1$ . We have not found it necessary to repeat this procedure iteratively. The three lowest signals in each panel of Figure 4 show the mean cross-talk in the demodulated channels after applying the refined  $\mathbf{D}'$  instead of the integer-only  $\mathbf{D}$ . This correction reduces the cross-talk between channels from the 1% level to only a few times  $10^{-4}$ .

### 3.2 Other sources of cross-talk

Even properly estimated,  $\mathbf{D}$  can remove cross-talk only if it is proportional to the primary pulse. Some forms of cross-talk, including a time-offset effect and magnetic coupling, are proportional to the time derivative of a pulse. If all cross-talk can be reduced to a level much lower than the TES energy resolution, then an array can operate at high photon rates with no degradation due to cross-talk.

The time-offset effect stems from the fact that the  $N$  modulated signals (upper panel of Figure 2) are measured not simultaneously but in succession over some 1 to  $10 \mu\text{s}$ . This is not ideal when one of the input signals changes rapidly, as at the beginning of a photon pulse. The time offset effect can be greatly reduced by linearly interpolating all modulated data streams between their actual sample times to estimate their values at the reference time, which is the same for all channels. We apply this “in-frame linear time correction” to all data shown in this report be-

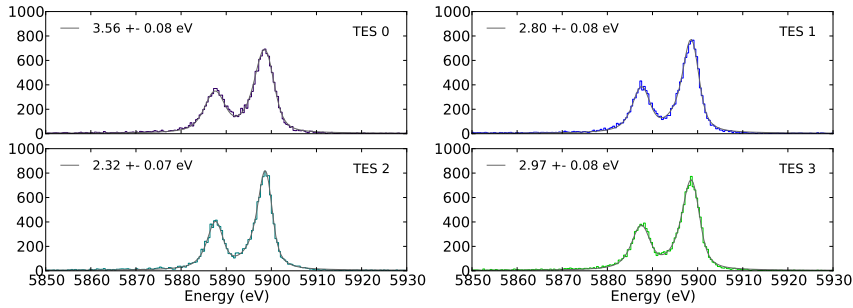


**Fig. 5** (Color online) The measured energy distributions of Mn  $K\alpha$  fluorescence (histograms) and the best fit distributions (smooth curves) assuming Gaussian-distributed resolutions of the given full width at half-maximum. The TESs are read out through a 4-channel flux-summing CDM. Vertical units are photons per 0.4 eV-wide bin. TES 0 is the unmodulated device and is expected not to perform as well as the others.

fore applying (or estimating) the demodulation  $\mathbf{D}$ , markedly reducing the size of the remaining cross-talk during the  $\sim 100\mu\text{s}$  rising edge of each pulse. Although the linear assumption can be generalized to higher orders through the approach of Savitzky-Golay filtering<sup>11</sup>, we find quadratic time correction not to be useful in the current system. The most important departure from linearity is the corner in the signal at the pulse onset, which higher-order polynomials do not model well.

Even with the corrections described so far, cross-talk in a form proportional to the time derivative of a pulse remains a concern. It probably results from magnetic coupling between channels and is just strong enough to limit the energy resolution at high photon rates. Research continues on this cross-talk mechanism and on how to mitigate it in hardware and in later analysis.

### 3.3 Performance of the multiplexed microcalorimeters

The proof of detector and multiplexer performance is the energy resolution achieved in real measurements; we employed the manganese fluorescence lines at 5.9 keV to estimate our detector resolutions. Typical observations involved one to ten photons per second per TES detector and lasted up to three hours. After making the corrections described above, we processed triggered data records roughly 15 ms long with optimal filtering<sup>12</sup> and a simple drift-correction proportional to variations in the baseline (pre-triggered) signal level of each TES.

We have found that the simplest method of fitting measured energy distribution to the expected line shape—by minimizing Pearson’s  $\chi^2$ —produces results biased towards lower (better) energy resolution. We therefore always perform a full maximum-likelihood fit to estimate energy resolutions, taking account of the Poisson-distributed nature of counts in a histogram.<sup>13</sup> For the data shown here with  $\sim 10^4$  photons per histogram, use of the maximum-likelihood fit makes the FWHM energy resolution approximately 0.05 eV worse than the  $\chi^2$  biased fit does. A larger bias is found when fewer photons are measured.

Figure 5 shows the best energy resolution accomplished over a long observation. The raw photon rate of 3.6 Hz per detector was maintained for 130 minutes. Each histogram contains between 17,000 and 18,000 photons in the Mn  $K\alpha$  energy range depicted, after all data-quality cuts. As expected, the three modulated detectors have better energy resolutions than TES 0. Their mean resolution of 2.70 eV exactly matches the mean resolution we have achieved through TDM with eight identical detectors in the same cryostat. For these spectra, we have vetoed records in which more than one of the four detectors are hit, as cross-talk remains just large enough to have an impact on resolution. This cross-talk cut improves the energy resolutions by 0.05 eV on average while removing some 15% of the records. In experiments with higher photon rates, the improvement in resolution with the cut is larger, but the price paid in lost data is also larger. Further reduction of cross-talk is vital to future high-rate experiments.

#### 4 Future directions

The CDM demonstration chip used in the present experiments also contains an eight-channel multiplexer, which we will test in the near future. In addition, a 32-channel device has been fully designed. Reaching higher multiplexing factors will require improved techniques for minimizing cross-talk between calorimeters.

A further development that promises to allow in-focal-plane multiplexing and a greatly reduced wire count is the current-summed CDM.<sup>14</sup> In that concept, the TES current polarity is modulated by SQUID-based superconducting double-pole double-throw switches. This approach allows the CDM basis functions to be stored in firmware rather than being patterned onto the SQUID chip. It is also compatible with microwave multiplexing.

We plan to use CDM as a simple upgrade for TDM readout systems, with significantly better performance at high multiplexing factors. These results show that the demonstration device with our current analysis techniques achieves energy resolutions as good as those found in similar detectors operated through TDM.

#### References

1. K. D. Irwin, *Appl. Phys. Lett.* **66**, 1998, (1995).
2. D. S. Swetz, et al., *Astrophys. J. Suppl.* **194**, 41, (2011).
3. J. E. Carlstrom, et al., *PASP* **123**, 903, (2011).
4. J. A. Chervenak, et al., *Appl. Phys. Lett.* , **74**, 4043, (1999).
5. M. F. Cunningham, et al., *Appl. Phys. Lett.* , **81**, 159, (2002).
6. B. S. Karasik & W. R. McGrath, *12th Symp. Space THz Tech.*, 436 (2001).
7. M. Podt, J. Weenink, J. Flokstra, & H. Rogalla, *Physica C* **368**, 218, (2002).
8. K.D. Irwin, et al., *Supercond. Sci. Technol.* **23**, 034004, (2010).
9. J. L. Walsh, *Am. J. Math.*, **45**, 5 (1923).
10. G. Hölzer, et al., *Phys. Rev.*, **A56**, 4554 (1997). F. S. Porter, private comm.
11. W. H. Press, et al., *Numerical Recipes, 3rd Edition*, Cambridge (2007).
12. B. Alpert, et al., *Proc. LTD-14*, (2011).
13. T. A. Laurence & B. A. Chromy, *Nature Meth.*, **7**, 338, (2010).
14. K. D. Irwin, et al., *Proc. LTD-14*, (2011).

J. W. Fowler<sup>1</sup>, W. B. Doriese<sup>1</sup>, G. Hilton<sup>1</sup>,  
K. Irwin<sup>1</sup>, D. Schmidt<sup>1</sup>, G. Stiehl<sup>1</sup>, D. Swetz<sup>1</sup>,  
J. N. Ullom<sup>1</sup>, and L. Vale<sup>1</sup>

# Optimization and analysis of code-division multiplexed TES microcalorimeters

22.07.2011

**Keywords** SQUID multiplexers, transition edge sensors

**Abstract** We are developing code-division multiplexing (CDM) systems for TES arrays with the goal of reaching multiplexing factors in the hundreds. We report on x-ray measurements made with a four-channel prototype CDM system that employs a flux-summing architecture, emphasizing data-analysis issues. We describe an empirical method to determine the demodulation matrix that minimizes cross-talk. This CDM system achieves energy resolutions of between 2.3 eV and 3.0 eV FWHM at 5.9 keV.

PACS numbers: 85.25.Dq, 85.25.Oj

## 1 Introduction

Transition-edge sensors<sup>1</sup> (TESs) are used in many different applications to sense photons over an enormous energy range. They are the leading detector technology in millimeter-wave and submillimeter astronomy, where focal planes of thousands of sensors have been fielded<sup>2,3</sup> and show great promise for astronomical x-ray spectroscopy. In the laboratory, TES devices have achieved the best energy resolution of any non-dispersive device for single photons in the gamma and x-ray bands—better than one part in one thousand.

One critical technology for building arrays of thousands of detectors has been cryogenic signal multiplexing, which reduces the number of electrical connections between stages at different temperatures by allowing multiple detectors to share

---

1:Quantum Sensors Project, National Institute of Standards and Technology, 325 Broadway MS 817.03, Boulder, CO 80305, USA

Tel: +1 303-497-3990

E-mail: joe.fowler@nist.gov

*Official contribution of the National Institute of Standards and Technology; not subject to copyright in the United States.*



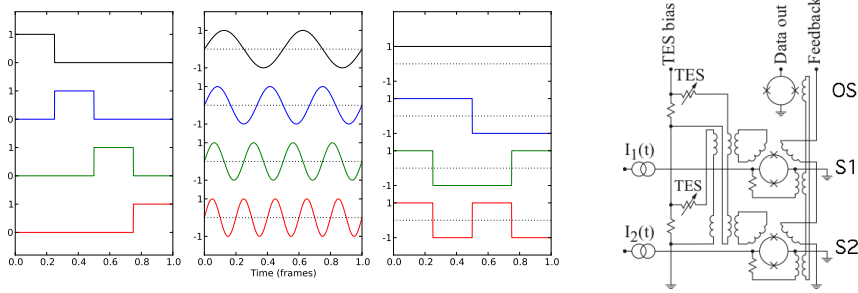


**Fig. 1** (Color online) *Left*: Three sets of orthogonal basis functions for multiplexing four pixels: time-division (boxcars), frequency-division (sinusoids), and code-division (Walsh codes). In each multiplexing scheme, the four detector outputs are multiplied by one of the four given modulation functions. *Right*: A two-channel code-division multiplexer that uses flux summation. Labels “OS”, “S1”, and “S2” refer to the output SQUID and SQUID switches 1 and 2. The magnetic flux in SQUID switch 1 is proportional to the sum of the two TES currents, while the flux in switch 2 is proportional to their difference (indicated by the oppositely-oriented inductors). When current is applied at either  $I_1(t)$  or  $I_2(t)$ , the output SQUID couples to either the sum or the difference of TES currents. We report on this CDM design, generalized to four TES detectors and an equal number of SQUID switches.

wiring. As future projects grow to larger device counts and employ faster detectors, they will require new multiplexing techniques to minimize both readout noise and instrument complexity.

Two multiplexing schemes currently used with TES arrays are time-division multiplexing (TDM)<sup>4</sup> and frequency-division multiplexing (FDM).<sup>5</sup> In this work, we present the first x-ray measurements with TES microcalorimeters read out with code-division multiplexing (CDM). This multiplexing approach combines many advantages of the other two, as argued in earlier works.<sup>6,7</sup> Figure 1 (left panel) compares the modulation functions used in TDM, FDM, and CDM for a four-channel system. In TDM, one detector is coupled to the output at a time. In CDM, all detectors are coupled at all times—with time-varying signs—removing the “multiplex disadvantage” of TDM, in which the aliased SQUID noise increases as the square root of  $N$ , the number of multiplexed detectors. CDM therefore has the potential to permit higher device speed, or to increase the number of devices multiplexed on one line, or both. We describe the design and characterization of a four-channel prototype and demonstrate that the energy resolution achieved while measuring 5.9 keV x-rays matches the resolution achieved through TDM readout.

## 2 A 4-channel CDM demonstration system

We have measured x-rays with microcalorimeters optimized for the 1 to 10 keV energy range, read out through a demonstration chip fabricated at NIST containing a four-channel CDM circuit. The code-division multiplexer operates by the principle of flux summation.<sup>8</sup> The right panel of Figure 1 shows a simplified two-channel model of the multiplexer. As in a TDM system,  $N$  detectors couple their current into  $N$  switching SQUIDs, whose outputs are summed by a single output SQUID. In a TDM system, the detectors and switching SQUIDs are paired so that

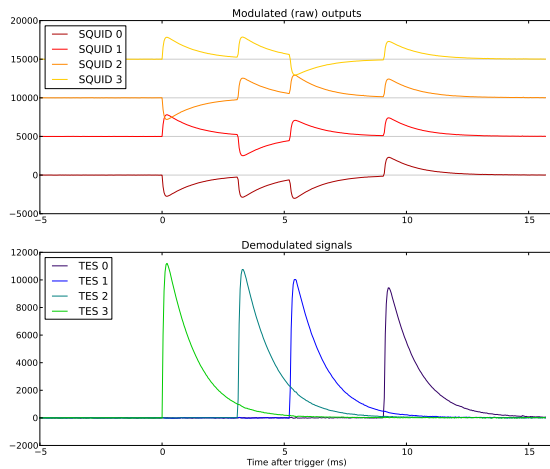


**Fig. 2** (Color online) Sample data from observing manganese fluorescence light for 21 ms. The raw data from the four SQUID switches (*top*) and the same data demodulated to recover the current from each of the four TES detectors (*bottom*) are shown. The vertical scale is arbitrary; the upper panel offsets each curve for clarity. This unusual time interval was selected to demonstrate all four modulations in one figure; only a small fraction of pulse records contain even two photons coinciding in such a short window.

each detector couples into only one switching SQUID; in the CDM system, all  $N$  detectors couple into all  $N$  SQUIDs, each detector having a different pattern of positive and negative couplings. For an appropriate set of  $N^2$  coupling polarities, the detectors' patterns are mutually orthogonal over the period required to read all  $N$  switching SQUIDs. The Walsh functions<sup>9</sup> provide one such basis.

The TDM and flux-summed CDM systems are used identically; in both, the  $N$  SQUID switches are activated singly in rapid succession. We can therefore use CDM chips as drop-in replacements for the TDM, with identical warm electronics to multiplex the signals. This interchangeability has enabled both rapid testing of the CDM prototype and direct comparisons of CDM with TDM results.

### 3 Characterization of the CDM data

We used CDM to read out a TES array measuring x-rays emitted by a manganese target bombarded with wide-band brehmsstrahlung radiation. Manganese fluoresces with a pair of  $K\alpha$  lines<sup>10</sup> at 5.9 keV separated by 11.1 eV. We estimate the energy resolution of the calorimeters from the observed line shapes.

Figure 2 shows a brief excerpt of the data from the 4-channel CDM system. The top panel shows the raw data as recorded by the system, one record from each of the four switching SQUIDs. They have been modulated by the Walsh functions designed into the CDM chip. Inversion of the Walsh coding yields the separate TES currents—as shown in the bottom panel of Figure 2.

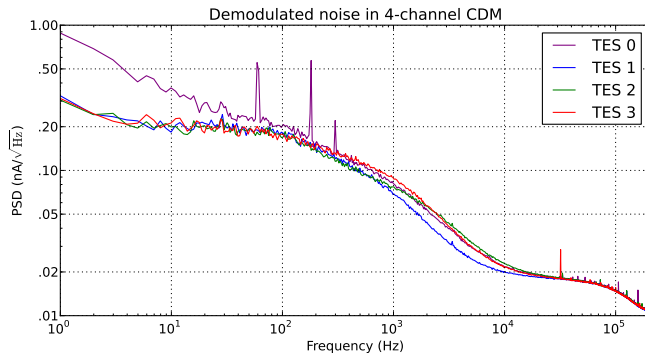


**Fig. 3** (Color online) The square root of the noise power spectral density in demodulated four-channel CDM data, averaged over 90 seconds with no x-ray sources. TES 0—the one unmodulated detector—has the highest noise level below 200 Hz, owing to gain drifts in second and third stage SQUIDs and pickup of the 60 Hz AC power line frequency (and at two odd harmonics). Modulation by Walsh functions removes most of this extra noise from the signal band in the other detector channels. The in-frame linear time correction described in Section 3.2 suppresses noise above 100 kHz in all channels.

One advantage of modulation by Walsh functions is that all but one detectors’ signals are differenced at multiples of the modulation frequency. Upon demodulation, low-frequency drifts and noise at the AC power line frequency and its overtones are moved out of the signal band, provided their source is upstream of the modulator (such as in the warm electronics). This effect can be seen in Figure 3, where only TES 0 (the unmodulated device) has excess noise below 100 Hz.

### 3.1 Solving for the demodulation matrix

One challenge in CDM is computation of the true demodulation matrix  $\mathbf{D}$  required to find the current through each of the  $N$  detectors given the  $N$  multiplexed outputs. We define  $D_{ij}$  as the contribution of the current from TES  $i$  to output channel  $j$ . By design, this matrix consists entirely of  $+1$  and  $-1$  elements:

$$\mathbf{D} = \begin{bmatrix} 1 & 1 & 1 & 1 \\ -1 & 1 & 1 & -1 \\ -1 & -1 & 1 & 1 \\ -1 & 1 & -1 & 1 \end{bmatrix} \quad (1)$$

In flux-summed CDM, the modulation coefficients are wired into the design by the lithographic traces in the multiplexer and cannot be adjusted after fabrication. Because the exact couplings depend on details of the SQUID switches and the geometry of the coils that convert current into magnetic flux,  $\mathbf{D}$  differs somewhat from its design value. We estimate the matrix empirically and have found that it is consistent over many weeks of operation. When needed, it can be computed from any sufficiently long calibration data set.

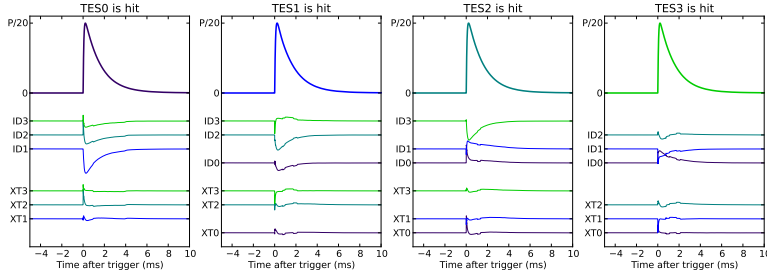


**Fig. 4** (Color online) Reduction in cross-talk through refining the demodulation matrix. Each panel shows the pulses caused by the TES cited at the top. The highest curve shows the pulse shape for the primary signal, scaled down by a factor of 20 for better comparison to cross-talk. Below this, three curves labeled “ID” show the unwanted cross-talk response in the *other* three channels, assuming an integer-only demodulation matrix. The lowest three curves show the cross-talk (“XT”) when the empirically derived demodulation is applied instead.

We refine our estimate of  $\mathbf{D}$ , starting from the integer-only matrix (Equation 1). The data required for the refinement are the mean current signals  $s_{ij}(t)$  from demodulated channel  $i$  when device  $j$  (and no other) is hit with a photon, plus the noise power spectrum  $n_j$  of each device. Figure 4 shows an example of all sixteen signals with the  $i = j$  cases plotted in the top of each panel and the twelve cross-talk ( $i \neq j$ ) cases below. The sampled functions of time are each converted to single values by the usual process of optimal filtering. A correction matrix  $\mathbf{C}$  is built from the filtered values:  $C_{ij}$  is the response in channel  $i$  to a photon hitting detector  $j$ . The correction  $\mathbf{C}$  will be close to the identity if  $\mathbf{D}$  was a good initial estimate. The revised demodulation matrix is then  $\mathbf{D}' = \mathbf{C}^{-1} \mathbf{D}$ . In practice, we find that elements of  $\mathbf{D}'$  are generally within 1% of  $\pm 1$ . We have not found it necessary to repeat this procedure iteratively. The three lowest signals in each panel of Figure 4 show the mean cross-talk in the demodulated channels after applying the refined  $\mathbf{D}'$  instead of the integer-only  $\mathbf{D}$ . This correction reduces the cross-talk between channels from the 1% level to only a few times  $10^{-4}$ .

### 3.2 Other sources of cross-talk

Even properly estimated,  $\mathbf{D}$  can remove cross-talk only if it is proportional to the primary pulse. Some forms of cross-talk, including a time-offset effect and magnetic coupling, are proportional to the time derivative of a pulse. If all cross-talk can be reduced to a level much lower than the TES energy resolution, then an array can operate at high photon rates with no degradation due to cross-talk.

The time-offset effect stems from the fact that the  $N$  modulated signals (upper panel of Figure 2) are measured not simultaneously but in succession over some 1 to 10  $\mu\text{s}$ . This is not ideal when one of the input signals changes rapidly, as at the beginning of a photon pulse. The time offset effect can be greatly reduced by linearly interpolating all modulated data streams between their actual sample times to estimate their values at the reference time, which is the same for all channels. We apply this “in-frame linear time correction” to all data shown in this report be-

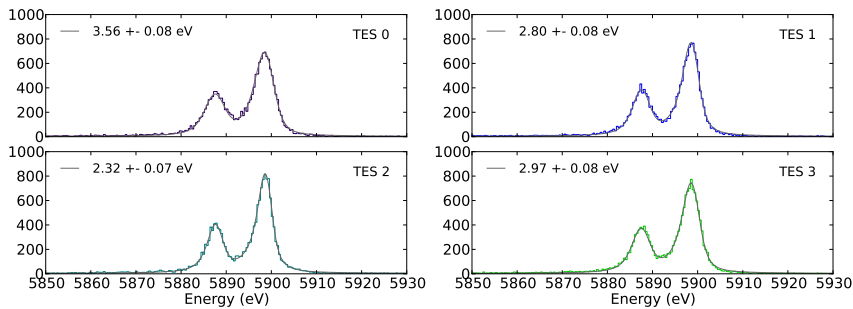


**Fig. 5** (Color online) The measured energy distributions of Mn  $K\alpha$  fluorescence (histograms) and the best fit distributions (smooth curves) assuming Gaussian-distributed resolutions of the given full width at half-maximum. The TESs are read out through a 4-channel flux-summing CDM. Vertical units are photons per 0.4 eV-wide bin. TES 0 is the unmodulated device and is expected not to perform as well as the others.

fore applying (or estimating) the demodulation  $\mathbf{D}$ , markedly reducing the size of the remaining cross-talk during the  $\sim 100 \mu\text{s}$  rising edge of each pulse. Although the linear assumption can be generalized to higher orders through the approach of Savitzky-Golay filtering<sup>11</sup>, we find quadratic time correction not to be useful in the current system. The most important departure from linearity is the corner in the signal at the pulse onset, which higher-order polynomials do not model well.

Even with the corrections described so far, cross-talk in a form proportional to the time derivative of a pulse remains a concern. It probably results from magnetic coupling between channels and is just strong enough to limit the energy resolution at high photon rates. Research continues on this cross-talk mechanism and on how to mitigate it in hardware and in later analysis.

### 3.3 Performance of the multiplexed microcalorimeters

The proof of detector and multiplexer performance is the energy resolution achieved in real measurements; we employed the manganese fluorescence lines at 5.9 keV to estimate our detector resolutions. Typical observations involved one to ten photons per second per TES detector and lasted up to three hours. After making the corrections described above, we processed triggered data records roughly 15 ms long with optimal filtering<sup>12</sup> and a simple drift-correction proportional to variations in the baseline (pre-triggered) signal level of each TES.

We have found that the simplest method of fitting measured energy distribution to the expected line shape—by minimizing Pearson’s  $\chi^2$ —produces results biased towards lower (better) energy resolution. We therefore always perform a full maximum-likelihood fit to estimate energy resolutions, taking account of the Poisson-distributed nature of counts in a histogram.<sup>13</sup> For the data shown here with  $\sim 10^4$  photons per histogram, use of the maximum-likelihood fit makes the FWHM energy resolution approximately 0.05 eV worse than the  $\chi^2$  biased fit does. A larger bias is found when fewer photons are measured.

Figure 5 shows the best energy resolution accomplished over a long observation. The raw photon rate of 3.6 Hz per detector was maintained for 130 minutes. Each histogram contains between 17,000 and 18,000 photons in the Mn  $K\alpha$  energy range depicted, after all data-quality cuts. As expected, the three modulated detectors have better energy resolutions than TES 0. Their mean resolution of 2.70 eV exactly matches the mean resolution we have achieved through TDM with eight identical detectors in the same cryostat. For these spectra, we have vetoed records in which more than one of the four detectors are hit, as cross-talk remains just large enough to have an impact on resolution. This cross-talk cut improves the energy resolutions by 0.05 eV on average while removing some 15% of the records. In experiments with higher photon rates, the improvement in resolution with the cut is larger, but the price paid in lost data is also larger. Further reduction of cross-talk is vital to future high-rate experiments.

#### 4 Future directions

The CDM demonstration chip used in the present experiments also contains an eight-channel multiplexer, which we will test in the near future. In addition, a 32-channel device has been fully designed. Reaching higher multiplexing factors will require improved techniques for minimizing cross-talk between calorimeters.

A further development that promises to allow in-focal-plane multiplexing and a greatly reduced wire count is the current-summed CDM.<sup>14</sup> In that concept, the TES current polarity is modulated by SQUID-based superconducting double-pole double-throw switches. This approach allows the CDM basis functions to be stored in firmware rather than being patterned onto the SQUID chip. It is also compatible with microwave multiplexing.

We plan to use CDM as a simple upgrade for TDM readout systems, with significantly better performance at high multiplexing factors. These results show that the demonstration device with our current analysis techniques achieves energy resolutions as good as those found in similar detectors operated through TDM.

#### References

1. K. D. Irwin, *Appl. Phys. Lett.* **66**, 1998, (1995).
2. D. S. Swetz, et al., *Astrophys. J. Suppl.* **194**, 41, (2011).
3. J. E. Carlstrom, et al., *PASP* **123**, 903, (2011).
4. J. A. Chervenak, et al., *Appl. Phys. Lett.* , **74**, 4043, (1999).
5. M. F. Cunningham, et al., *Appl. Phys. Lett.* , **81**, 159, (2002).
6. B. S. Karasik & W. R. McGrath, *12th Symp. Space THz Tech.*, 436 (2001).
7. M. Podt, J. Weenink, J. Flokstra, & H. Rogalla, *Physica C* **368**, 218, (2002).
8. K.D. Irwin, et al., *Supercond. Sci. Technol.* **23**, 034004, (2010).
9. J. L. Walsh, *Am. J. Math.*, **45**, 5 (1923).
10. G. Hölzer, et al., *Phys. Rev.*, **A56**, 4554 (1997). F. S. Porter, private comm.
11. W. H. Press, et al., *Numerical Recipes, 3rd Edition*, Cambridge (2007).
12. B. Alpert, et al., *Proc. LTD-14*, (2011).
13. T. A. Laurence & B. A. Chromy, *Nature Meth.*, **7**, 338, (2010).
14. K. D. Irwin, et al., *Proc. LTD-14*, (2011). arXiv:1110.1608